Journal of Applied Physics ARTICLE scitation.org/journal/jap

Reducing Shockley–Read–Hall recombination losses in the depletion region of a solar cell by using a wide-gap emitter layer

Cite as: J. Appl. Phys. **130**, 153102 (2021); doi: 10.1063/5.0060158
Submitted: 15 June 2021 · Accepted: 24 September 2021 ·
Published Online: 18 October 2021

Tetsuya Nakamura,[1,a)] Warakorn Yanwachirakul,[2] Mitsuru Imaizumi,[1] Masakazu Sugiyama,[3] Hidefumi Akiyama,[4,5] and Yoshitaka Okada[3]

AFFILIATIONS

[1]Japan Aerospace Exploration Agency, 2-1-1 Sengen, Tsukuba, Ibaraki 305-8505, Japan
[2]Department of Electrical Engineering and Information Systems, Graduate School of Engineering, The University of Tokyo, 7-3-1 Hongo, Bunkyo-ku, Tokyo 113-8654, Japan
[3]Research Center for Advanced Science and Technology, The University of Tokyo, 4-6-1 Komaba, Meguro-ku, Tokyo 153-8904, Japan
[4]Institute for Solid State Physics, The University of Tokyo, 5-1-5 Kashiwanoha, Kashiwa, Chiba 277-0882, Japan
[5]AIST-UTokyo OPERANDO-OIL, The University of Tokyo, 5-1-5 Kashiwanoha, Kashiwa, Chiba 277-0882, Japan

[a)]**Author to whom correspondence should be addressed:** nakamura.tetsuya@jaxa.jp

ABSTRACT

The conversion efficiency of a solar cell depends on the degree of non-radiative recombination, and thus efficiency improvements can also be achieved by reducing Shockley–Read–Hall (SRH) recombination losses. This type of loss depends not only on the crystal quality, but also on the device structure. A clear separation of the contributions of these factors would improve our understanding of the control of non-radiative recombination. In this work, we discuss the reduction of the integrated SRH recombination rate in the depletion region ($U_{\mathrm{SRH}}^{\mathrm{dep}}$) by changing the emitter material, instead of fabricating a base layer with a higher crystal quality. First, we theoretically show that, by employing a suitable n-InGaP/p-GaAs heterojunction structure instead of a GaAs p–n homojunction, the integrated $U_{\mathrm{SRH}}^{\mathrm{dep}}$ can be reduced, because a significant part of the depletion region in the heterojunction is located in the wide-gap emitter material, which has a lower intrinsic carrier density. Then, the effective SRH recombination coefficient in the depletion region ($\overline{A^{\mathrm{dep}}}$) is obtained from experiments, and the effect of the structural modification on $U_{\mathrm{SRH}}^{\mathrm{dep}}$ is analyzed. We are able to clearly assess the effect of the heterojunction structure on the non-radiative recombination because the grown samples exhibit the same radiative recombination loss. The analysis reveals that, in suitable heterojunction solar cells with an emitter layer containing a low intrinsic carrier concentration, $\overline{A^{\mathrm{dep}}}$ (and thus also $U_{\mathrm{SRH}}^{\mathrm{dep}}$) is effectively reduced.

I. INTRODUCTION

The higher the conversion efficiency of a solar cell (η_{sc}), the more suitable the solar cell is for application areas with limited space. In particular, there have been efforts to make application areas such as automobiles more environmentally friendly by using high-efficiency solar cells.[1,2] In order to obtain sufficient power for a vehicle from attached solar panels, the improvement of η_{sc} is still an important issue.

In improving η_{sc}, it is helpful to consider the conversion loss, i.e., the difference between the actual efficiency of a given device and its theoretical efficiency limit. The concept of the internal radiative limit has been employed to determine the effective theoretical limits of non-idealized solar cells.[3] Here, the parameter of primary interest is the internal luminescence efficiency (η_{int}),[3,4] which is the probability of radiative electron–hole recombination. The radiative limit describes the condition where η_{int} is unity. It has been reported that GaAs solar cells can exhibit η_{int} values close to 100% under conditions where the recombination current (J_{rec}) is relatively high, that is, under conditions corresponding to the open-circuit

condition.[5] This means that the open-circuit voltage (V_{oc}) of such a GaAs solar cell has almost reached the internal radiative limit. On the other hand, the η_{int} values at relatively low J_{rec} values that correspond to the maximum power point are significantly lower than those at the open-circuit condition. This means that even in GaAs solar cells, there is still room for the improvement of the η_{int} at the maximum power point.[6] Since the effect of recombination in the depletion region is dominant in the low-J_{rec} regime,[6] it is important to reduce the Shockley–Read–Hall (SRH) recombination[7–9] rate in the depletion region (U_{SRH}^{dep}) (because this recombination is non-radiative). By reducing this SRH recombination, the η_{int} at the maximum power point can be improved, i.e., η_{sc} can be improved.

Most solar cells employ homojunctions, that is, a p–n junction composed of a single semiconductor material. Instead of improving the crystal quality of the homojunction material, it should also be possible to reduce the SRH recombination loss in the depletion region by changing the solar cell structure. To study the effect of the structural modification on the SRH recombination in a solar cell, the use of a heterojunction structure can be considered. The concept of using a heterojunction structure instead of a homojunction is well known, and it has been shown that using a heterojunction structure can have various positive effects on solar cells. For example, it can result in a surface passivation effect, which has contributed to the realization of high-efficiency Si solar cells.[10] It has also been reported that defects such as deep-donor levels (DX-centers) can be avoided by using a heterojunction structure: By using an n-InGaP emitter (bandgap energy $E_g \approx 1.9$ eV) instead of n-$Al_{0.28}Ga_{0.72}As$ ($E_g \approx 1.8$ eV), the V_{oc} can be improved compared to an $Al_{0.28}Ga_{0.72}As$ homojunction solar cell[11] since the DX-center density in n-InGaP is lower than that in n-$Al_{0.28}Ga_{0.72}As$.[12] Furthermore, it is also possible to reduce both radiative and non-radiative recombination losses by using a wide-gap material: Ragay *et al.* showed that adding an i-layer of $Al_{0.05}Ga_{0.95}As$ ($E_g \approx 1.49$ eV) in a GaAs ($E_g \approx 1.42$ eV) solar cell reduces the dark current compared to a GaAs homojunction solar cell.[13] Since the emission of $Al_{0.05}Ga_{0.95}As$ was confirmed in addition to the emission of GaAs, the splitting of the quasi-Fermi levels in the $Al_{0.05}Ga_{0.95}As$ layer was larger than that in the neighboring GaAs layers, which implies a reduction of radiative and non-radiative recombination losses. Similarly, Steiner *et al.* reported emission from the wide-gap and base materials and the reduction of the saturation dark current in an $Al_{0.18}In_{0.49}Ga_{0.33}P$/InGaP heterojunction solar cell.[14] Because the theoretical efficiency limit assumes only radiative recombination loss, such reductions in the radiative recombination loss by using the heterojunction design imply that the theoretical efficiency limit changes, which makes a quantitative comparison of the effect of the device design on the non-radiative recombination more difficult. Although several studies on rear-heterojunction solar cells, which have a thick base layer with a narrow-gap material at the front side and a thin emitter layer with a wide-gap material at the back side, suggest a reduction of non-radiative recombination,[15,16] assessing the correlation between the splitting of the quasi-Fermi levels in the wide-gap material and the narrow-gap material is difficult since it is difficult to measure the emission of the wide-gap material due to the absorption by the narrow-gap material. To the best of our knowledge, there are not many experiments that can clearly separate the various effects of a heterojunction structure. For example, a quantitative assessment of the effect of reducing the non-radiative recombination loss in the depletion region by using a heterojunction structure without changing the base layer design, absorption properties, and the radiative recombination has not yet been presented.

Note that in order to quantitatively analyze the SRH recombination loss in the depletion region of heterojunction solar cells, there are two technical issues. One is to separate the effects of the two materials on the output voltage, i.e., the contribution of the E_g of each material to the quasi-Fermi-level splitting. The other is to derive the characteristics of the SRH recombination in the depletion region. Regarding the first issue, it is possible to investigate the effect of each material (with different E_g) on the output voltage by a quantitative electroluminescence (EL) spectrum analysis[17] if the reciprocity relation between EL and external quantum efficiency (EQE)[18] is established in the investigated heterojunction solar cells. For the second issue, the well-known AB model,[6] which is derived from carrier-recombination rate equations and is helpful to analyze active layers in light-emitting diodes,[19] can be applied to obtain the effective SRH recombination coefficient in the depletion region of the heterojunction solar cell.

In this study, we theoretically show that, compared to a GaAs p–n homojunction, an n-InGaP/p-GaAs front-heterojunction solar cell structure, which has the emitter layer with the wide-gap material at the front side and the base layer with the narrow-gap material at the back side, can exhibit a lower integrated U_{SRH}^{dep}. In addition, we actually fabricate such solar cells by metal organic chemical vapor deposition (MOCVD) and quantitatively analyze their EL spectra and their effective SRH recombination coefficients in the depletion region in GaAs, $\overline{A^{dep}}$. Based on the simulations and experiments, we are able to quantitatively discuss the reduction of the SRH recombination loss in the depletion region that occurs by employing a heterojunction structure.

II. CALCULATION

In this section, we consider the characteristics that control the carrier density at the position where the electron density (n) and the hole density (p) are equal in the depletion region of a heterojunction structure. This position is hereafter referred to as x^{eq}, and n and p at the position x^{eq} are denoted by n^{dep} and p^{dep}, respectively. According to Eq. (1), the SRH recombination rate U_{SRH} reaches its maximum at x^{eq},

$$U_{SRH} \approx \frac{pn - n_i^2}{(n + n_i)\tau_{SRH}^p + (p + n_i)\tau_{SRH}^n}. \quad (1)$$

Here, n_i is the intrinsic carrier density and τ_{SRH}^p and τ_{SRH}^n are the SRH lifetimes of the holes in the n-layer and the electrons in the p-layer, respectively. This equation assumes that the trap level is equal to the intrinsic Fermi level. The parameter n^{dep} can be expressed in terms of n_i, the elementary charge q, the applied bias voltage V, the Boltzmann constant k, and the absolute temperature T of the device,

$$n^{dep} = n_i \exp\left(\frac{qV}{2kT}\right). \quad (2)$$

Since n^{dep} at a given T is determined by n_i and V, the maximum value of U_{SRH} in a homojunction solar cell under V cannot be reduced as long as we do not take measures to increase τ^p_{SRH} and τ^n_{SRH}, that is, as long as the material quality does not change. On the other hand, in the case of a heterojunction solar cell that uses a wide-gap material with a relatively low n_i for the emitter layer, the maximum value of U_{SRH} can be reduced without increasing τ^p_{SRH} and τ^n_{SRH} since the position x^{eq} and the value of n^{dep} can be controlled by choosing a suitable heterojunction structure. Before we explain the simulation results, we briefly explain why our simulations use the approximation that the SRH lifetime is independent of the doping concentration of the emitter layer. In the case of a heterojunction solar cell, the U_{SRH} in the wide-gap material is negligible compared to that in the narrow-gap material because the minority carrier density in the wide-gap material is low if the quasi-Fermi-level splitting is constant throughout the junction (this condition is satisfied in our samples as shown later). In a heterojunction solar cell with a doping concentration of $2 \times 10^{17}\,cm^{-3}$ in the emitter layer, of which this value is close to the experimental results described in Sec. IV, the U_{SRH} in the wide-gap material is more than 10^4 times smaller than that in the narrow-gap material. Therefore, even if the lifetime of the wide-gap material changes significantly, its effect can be ignored. In the case of a homojunction solar cell, a doping-concentration-dependent SRH lifetime directly affects U_{SRH}. For simplicity, we also assumed a constant SRH lifetime for the GaAs emitter, but we chose a sufficiently long lifetime for GaAs emitter in order to compare the effects of the doping concentration on U_{SRH}.

First, we compare the U_{SRH} values calculated for a GaAs homojunction solar cell and several n-InGaP/p-GaAs heterojunction solar cells by using the solar cell simulation software PC1D.[20] To identify the degree of n^{dep} of a heterojunction solar cell, the dependency of U_{SRH} on the doping concentration in the n-type emitter layer ($n^{emitter}$) was calculated without changing the doping concentration in the p-type base layer (p^{base}). The surface recombination rate was set to zero to clarify the influence of the recombination in the depletion region (the validity of this assumption is shown in Sec. IV). Table I shows the detail of each simulated solar cell structure. A typical heterojunction solar cell with a high η_{sc} has a base layer with a narrow-gap material and an emitter layer with a wide-gap material at the front and back sides, respectively.[15] However, this structure is not suitable for our study, because in such a device the η_{sc} is improved not only by the effect of using a heterojunction structure but also by the effect of photon recycling.[21] In addition, in the typical structure, it is difficult to measure the EL spectrum of the wide-gap material due to the absorption by the narrow-gap material at the front side. Therefore, we employed a structure with a wide-gap InGaP emitter layer at the front side and a narrow-gap GaAs base layer at the back side. As shown in Table I, our heterojunction solar cells contain an interface region consisting of a 2-nm-thick p-type GaAs layer. The simulations of the heterojunction solar cells were carried out with different carrier lifetimes in this GaAs volume adjacent to the heterointerface (hereafter referred to as Case 1, Case 2, and Case 3 as shown in Table I). The lifetime in this region can be lower than in GaAs bulk, because the formation of an intermixing (In)GaAs (P) may lead to strain-induced defects in this region. In a previous study using InGaP/GaAs quantum well structures, the effect of interfacial defects at the heterointerface was observed with a thickness of several nanometers.[22] Therefore, we assumed a thickness of 2 nm for this interface region. In order to enable a comparison with the experimental EL characteristics in the low-J_{rec} regime, the bias voltage used in the simulations was set to that value where $J_{rec} = 1\,mA/cm^2$ under dark condition. From the distributions of the carrier densities obtained in the simulation, the distribution of U_{SRH} was calculated using Eq. (1). The values of n_i in InGaP and GaAs were set to 1.2×10^3 and $1.79 \times 10^6\,cm^{-3}$, respectively.[17] Note that Table I indicates a range for the assumed $n^{emitter}$ values. In the simulations, we used 18 different values in the range from 1×10^{16} to $2 \times 10^{18}\,cm^{-3}$ to verify the influence of $n^{emitter}$.

TABLE I. Device properties used in the simulations.

		Homojunction	Heterojunction
Emitter (n)	Material	GaAs	InGaP
	n (cm^{-3})	1×10^{16}–2×10^{18}	1×10^{16}– 2×10^{18}
	Thickness (nm)	50	50
	Lifetime (μs)	1	0.1
Interface (p)	Material	N/A	GaAs
	p (cm^{-3})		1×10^{17}
	Thickness (nm)		2
	Lifetime (μs)		Case 1: 1
			Case 2: 0.1
			Case 3: 0.01
Base (p)	Material	GaAs	GaAs
	p (cm^{-3})	1×10^{17}	1×10^{17}
	Thickness (nm)	950	998
	Lifetime (μs)	1	1

Figure 1 shows the results of three different calculation conditions with respect to $n^{emitter}$; the left, middle, and right columns are for $n^{emitter} = 2 \times 10^{16}$, 2×10^{17}, and $2 \times 10^{18}\,cm^{-3}$, respectively. Each panel contains the data of the same four device structures (the homojunction reference cell and the heterojunctions for Cases 1–3) indicated by the black, red, green, and blue curves. Each row in Fig. 1 shows, from top to bottom, the calculation results for U_{SRH}, the carrier densities, and the band diagram. In the bottom row, the solid lines represent the conduction band minima and the valence band maxima, and the broken lines represent the quasi-Fermi levels of electrons and holes. Since the quasi-Fermi-level splitting in the wide-gap InGaP layer is the same as that in the narrow-gap GaAs layer, these heterojunctions can be regarded as GaAs solar cells. As can be confirmed in the top and middle rows, the U_{SRH} of the homojunction solar cell reaches its maximum at the position x^{eq}. In the case of the homojunction solar cell, the maximum values of U_{SRH} are the same independent of the $n^{emitter}$ condition, because the change in $n^{emitter}$ has no influence on the value of n^{dep}. For the heterojunction solar cell Case 1, we can confirm that the maximum U_{SRH} is smaller for lower emitter-doping levels. The detailed trends of all four device structures are explained using Fig. 2.

Figure 2 summarizes the $n^{emitter}$ dependences of the effective SRH recombination coefficient in the depletion region in GaAs, A^{dep}. We calculated this value using Eq. (3),

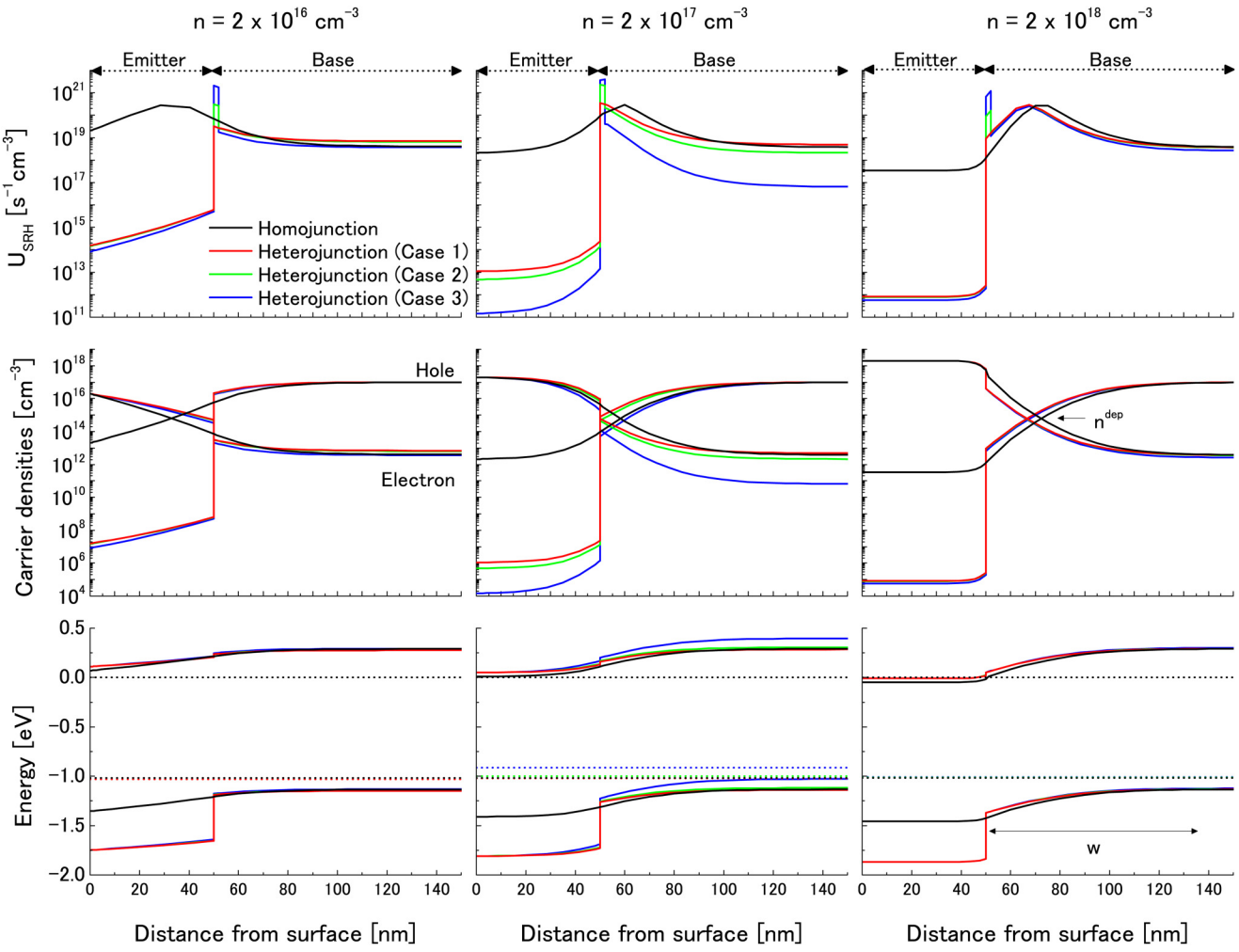

FIG. 1. Simulation results of the band diagram (bottom row), the carrier density distribution (middle row), and the SRH recombination rate distribution (top row). The bias voltage was applied to the value where $J_{rec} = 1\,mA/cm^2$ under dark condition. The left, center, and right columns correspond to the conditions $n^{emitter} = 2 \times 10^{16}$, 2×10^{17}, and $2 \times 10^{18}\,cm^{-3}$, respectively. The arrow for n^{dep} shows the value where n and p are equal (in the depletion region). The region denoted with w represents the width of the depletion region in the GaAs base layer where the spatial energy variation exceeds 1×10^{-4} eV/nm.

$$\overline{A^{dep}} \equiv \frac{\int_{x=x_0}^{x=x_0+w} U_{SRH}\,dx}{n^{dep} w}. \tag{3}$$

Here, x_0 is the position of the beginning of the depletion region in GaAs and w is the width of the depletion region in GaAs. For heterojunction cells, the U_{SRH} in the InGaP layer is negligible compared to that in the GaAs layer. The U_{SRH} in the InGaP layer is lower since the minority carrier density in the InGaP is much lower than that in the GaAs due to the difference in n_i. Thus, w of the heterojunction cell can be considerably included only the part existing in the GaAs which is indicated in the band diagram in Fig. 1. In this study, the depletion region is defined as the region where the spatial energy variation exceeds 1×10^{-4} eV/nm. The numerator and denominator of Eq. (3) are the contribution to U_{SRH}^{dep} from GaAs and the effective number of carriers in the depletion region, respectively. For a simple comparison, the vertical axis in Fig. 2 is normalized to the value obtained for $\overline{A^{dep}}$ of the homojunction solar cell with $n^{emitter} = 2 \times 10^{18}\,cm^{-3}$. Note that all four devices provide a nearly similar value of $\overline{A^{dep}}$ at $n^{emitter} = 2 \times 10^{18}\,cm^{-3}$. In the case of the homojunction solar cell (Fig. 2; cross symbols), $\overline{A^{dep}}$ is almost constant in the range from 2×10^{18} to $1 \times 10^{17}\,cm^{-3}$. The latter value is the doping concentration of the p-type base layer, p^{base}. By further reducing $n^{emitter}$, $\overline{A^{dep}}$ starts to increase since the depletion region spreads without changing the maximum value of U_{SRH} (see the black curves in the top row of Fig. 1). On the other hand, in Case 1 of the heterojunction solar cell, the $\overline{A^{dep}}$ decreases as $n^{emitter}$

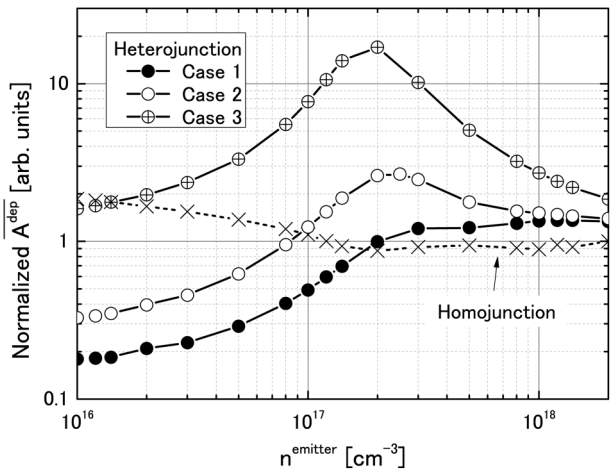

FIG. 2. Simulation results of the $n^{emitter}$ dependence of $\overline{A^{dep}}$ of GaAs. The y axis is normalized to the value obtained for $\overline{A^{dep}}$ of the GaAs homojunction device with $n^{emitter} = 2 \times 10^{18}$ cm^{-3}. The doping concentration of the p-type base layer (p^{base}) was set to 1×10^{17} cm^{-3}.

is reduced to values below p^{base} (see the closed circles in Fig. 2). In the regime of low $n^{emitter}$ values, the depletion region in Case 1 is formed not only in the GaAs base layer but also in the InGaP emitter layer (see the red curves in the bottom row of Fig. 1). The maximum value of U_{SRH} in the GaAs layer is significantly lower in the regime of low $n^{emitter}$ values where a large part of the depletion region is formed in the InGaP layer. Therefore, the heterojunction solar cell with the lowest $n^{emitter}$ has a smaller U_{SRH}^{dep} ($\propto \overline{A^{dep}}$) than the homojunction solar cell.

In the above simulation, the doping concentration and lifetime within each layer were assumed to exhibit no depth dependence within each layer. However, these parameters may change locally due to the effects of the heterointerface. In the following, the effect of local changes in the doping concentration and lifetime on $\overline{A^{dep}}$ is described. Regarding the doping concentration, the influence of a local change in $n^{emitter}$ on the distribution of p^{base} near the heterointerface is particularly large since the $\overline{A^{dep}}$ of the heterojunction structure is determined by the spatial extension of the depletion region defined by w and x_0, as shown in Case 1. Regarding the carrier lifetime, the lifetimes in the emitter and base layers have a small effect on the position of the depletion region (defined by w and x_0) as can be seen from the rather similar band diagrams of Case 1, Case 2, and Case 3 in Fig. 1. However, a local decrease in the lifetime directly affects $\overline{A^{dep}}$ according to Eq. (1). As shown in the top panel of the center column of Fig. 1, the U_{SRH} values of Cases 2 and 3 are relatively high at the heterointerface compared to Case 1. In Case 3, where the carrier lifetime in GaAs near the heterointerface is 1/100 of that in the base layer, $\overline{A^{dep}}$ reaches its maximum for $n^{emitter} = 2 \times 10^{17}$ cm^{-3} as shown in Fig. 2. The $\overline{A^{dep}}$ in Case 3 is higher than the reference homojunction structure even in the regime of low $n^{emitter}$ values, because the lifetime at the heterointerface is significantly shorter. In Case 2, where the lifetime in GaAs near the heterointerface is 1/10 of that in the base layer, $\overline{A^{dep}}$ can reach values that are lower than in the reference homojunction structure if $n^{emitter}$ is reduced sufficiently. These results suggest that a certain quality of the heterointerface is required to reduce $\overline{A^{dep}}$ by employing a heterojunction structure instead of a homojunction structure.

The radiative recombination rate (U_{rad}) of GaAs in the depletion region under a given bias voltage V is constant regardless of the emitter design since $U_{rad} = Bnp = Bn_i^2 \exp(qV/kT)$, where B is the radiative recombination coefficient. In addition, the U_{rad} of InGaP is negligible compared to that of GaAs at the same applied bias voltage. Therefore, by changing the structure of a solar cell from a homojunction to a heterojunction, it is possible to improve the average η_{int} of the whole cell, where $\eta_{int} = U_{rad}/(U_{rad} + U_{SRH})$.[6]

The simulation results indicate that U_{SRH}, $\overline{A^{dep}}$, and the average η_{int} of the whole cell can be improved by employing a heterojunction structure instead of a homojunction even if the material quality is the same as that of the homojunction. Note that a sufficiently long diffusion length in the base layer is necessary to realize a higher η_{sc} by the heterojunction structure since a drift effect cannot be expected in the neutral region.

III. EXPERIMENTAL DETAILS

Our simulation results for the n-InGaP/p-GaAs heterojunction solar cells in Sec. II suggested that the U_{SRH} and the $\overline{A^{dep}}$ of the GaAs base layer change depending on the doping concentration of the InGaP emitter layer. In order to confirm these simulation results experimentally, different heterojunction solar cells were fabricated by MOCVD (AIXTRON AIX200/4). We used a single GaAs homojunction design (reference cell) and five different n-InGaP/p-GaAs heterojunction designs (referred to as HJ #1–#5). Figure 3 presents the detail of device structures. The precursors for the crystal growth were trimethyl gallium (TMGa), trimethyl indium (TMIn), tertiary butyl arsine (TBAs), tertiary butyl phosphine (TBP), dimethyl zinc (DMZn), and hydrogen sulfide (H_2S). Zinc (Zn) and sulfur (S) were used as the p- and n-type dopants, respectively. The growth temperature and pressure were 610 °C and 100 mbar, respectively. The GaAs (001) wafers were used as substrates. A 100-nm-thick p-GaAs was grown on the substrate to smooth the surface. A 25-nm-thick p-$In_{0.49}GaP$ was next grown on the buffer as a back surface field (BSF) layer. For the homojunction solar cells, a p-GaAs base layer (950 nm), a n-GaAs emitter layer (50 nm), an n-$In_{0.49}GaP$ window layer (50 nm), an n-$In_{0.40}GaP$ window layer (10 nm), and an n^+-GaAs contact layer (50 nm) were grown on the BSF layer. For the heterojunction solar cells, a p-GaAs base layer (1000 nm), an n-$In_{0.49}GaP$ emitter layer, an n-$In_{0.40}GaP$ window layer (10 nm), and an n^+-GaAs contact layer (50 nm) were next grown on the BSF layer. Table II shows the growth conditions of the emitter layers. Since GaAs generally has longer diffusion lengths than InGaP,[23] the InGaP emitter layer should be thin from the viewpoint of carrier collection. However, in the case of a thin InGaP layer, it is difficult to reduce the doping concentration in the emitter layer volume near the heterointerface

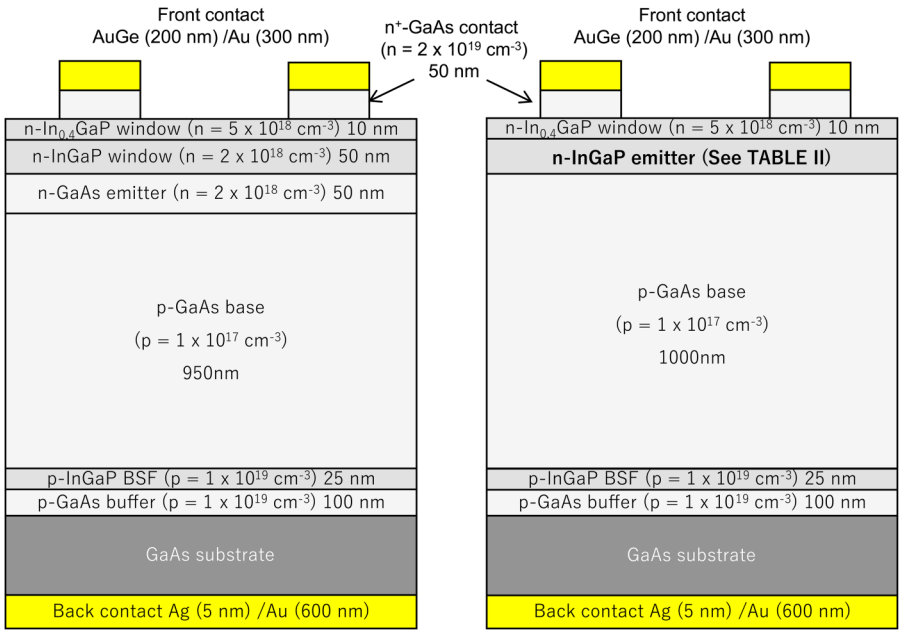

FIG. 3. Detailed structures of the solar cell devices grown by MOCVD (left: GaAs homojunction solar cell, right: InGaP/GaAs heterojunction solar cell).

only by controlling the H_2S partial pressure because of diffusion from the highly doped contact and window layers. Therefore, we aimed to reduce the doping concentration in the emitter layer not only by controlling the H_2S partial pressure but also by increasing the thickness of InGaP. Note that the design of the window layer of the homojunction is different from that of the heterojunction solar cells in order to make the thicknesses of the InGaP layers of the reference cell and HJ #1–#3 equal. All devices contain no antireflection coating and the solar cell device area was 1 cm^2 (1 cm × 1 cm). We measured the current–voltage (IV) characteristics under simulated AM1.5G illumination (1 sun) and also under dark conditions using a source and measurement unit (SMU). The former IV data are hereafter referred to as the light IV (LIV) and the latter referred to as the dark IV (DIV) characteristics. Additionally, we also measured the EQE, and EL spectra at 25 °C. The EL measurements were performed using an integrating sphere and a spectrometer with a cooled and calibrated Si CCD.[24] To understand the influence of the device structure on the SRH recombination, $\overline{A^{dep}}$ was used as a fitting parameter for the analysis of the average η_{int} of the whole cell volume, $\overline{\eta_{int}}$, using the AB model.[6]

The actual doping concentration profiles including the effects of diffusion were measured by secondary ion mass spectrometry (SIMS). The primary ion and the acceleration energy used for the SIMS measurement were Cs^+ and 3.0 kV, respectively. The uncertainty of the SIMS measurement without knock-on and matrix effects was ±40% (coverage factor K = 2). Since the prepared cells have layers with high sulfur concentration at the front side, the ion irradiation from this side may lead to the presence of the knock-on effect. In order to avoid this effect, the ion irradiation was

TABLE II. Emitter growth properties.

	Material	Thickness (nm)	Partial pressure of H_2S (mbar)
Ref.	GaAs	50	8.3×10^{-5}
HJ #1	InGaP	50	1.2×10^{-5}
HJ #2	InGaP	50	5.4×10^{-6}
HJ #3	InGaP	50	4.4×10^{-6}
HJ #4	InGaP	300	1.2×10^{-5}
HJ #5	InGaP	300	4.4×10^{-6}

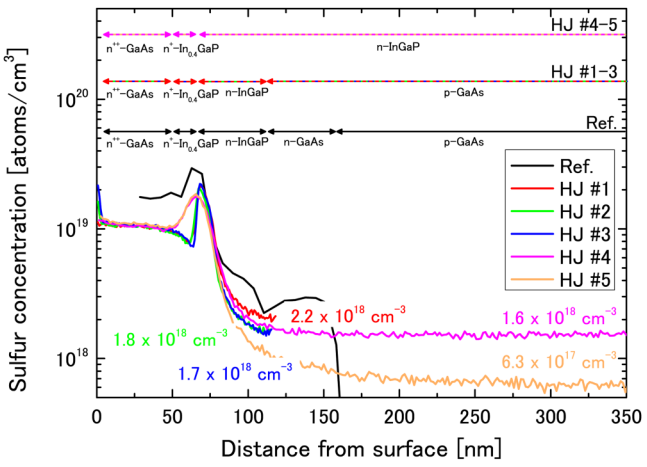

FIG. 4. Depth profiles of the sulfur concentration obtained by SIMS.

performed from the back side in the case of sulfur concentration measurements in the heterojunction solar cells.

IV. RESULTS AND DISCUSSION

Figure 4 plots the sulfur concentration profiles measured by SIMS. The average values of the sulfur concentration in the InGaP emitter layer near the heterointerface are indicated in the figure. Although the n-type layers of HJ #3 and HJ #5 were deposited under the same H_2S partial pressure, their sulfur concentrations near the heterointerface differ by a factor of about three. This large difference is presumably due to the diffusion of sulfur from the layers at the front side. The measured zinc concentration was about 1×10^{17} cm^{-3} for each base layer.

Figure 5 and Table III show the typical LIV curves of the fabricated cells and their output parameters, respectively. Two data sets are provided for each structure, corresponding to two devices fabricated from the same wafer. Regarding the short-circuit current density (J_{sc}), Fig. 5 clearly shows that the J_{sc} values of HJ #4 and HJ #5 are relatively low, which is attributed to the thick InGaP emitter layer (see also their EQE spectra in Fig. 6). The results also show that the V_{oc} values of HJ #1 and HJ #2 are lower than those of the two reference GaAs homojunction solar cells. On the other hand, the V_{oc} values of HJ #3, HJ #4, and HJ #5 are higher than those of the reference cells.

In the following discussion, we only compare the solar cells fabricated from the center region of the wafer to avoid the effects of inhomogeneity on thickness, dopant concentration, and crystal quality. Figure 6 shows the wavelength dependences of the EQE (solid curves) and the spectra of the absolute EL intensity (broken curves) of our devices. Although the design of the window layer of the reference cell is different from that of the heterojunction solar cells HJ #1–#3, their EQEs are almost the same. This indicates EQE seem to be saturated at the short-wavelength regime. Therefore, it is possible to compare the experimental results with the simulation results, which ignore the effects of surface recombination. In the short-wavelength regime, the EQEs of HJ #4 and HJ #5 with the thick InGaP layer are lower than those of the other devices. The fact that the ratio of the EQE of HJ #4 (or HJ #5) to that of HJ #1 (or HJ #2 or #3) decreases as the wavelength becomes shorter indicates that the diffusion length in n-InGaP is shorter than the thicknesses of InGaP in HJ #4 and HJ #5. One of the reasons for the shorter diffusion length is probably an imperfection of the n-InGaP. However, as mentioned in Sec. II, the quality of the InGaP emitter layer has almost no effect on U_{SRH}.

As shown in Fig. 6, all five devices have almost the same EQE near the band edge of GaAs. Therefore, the qualities of the GaAs base layers can be regarded as equivalent. Furthermore, all cells exhibit the same shape of the EL spectrum, and only emission from

TABLE III. Measured LIV parameters (AM1.5G, 25 °C, 1 sun). Two data sets are provided for each sample, corresponding to two devices fabricated from the same wafer.

	J_{sc} (mA/cm^2)	V_{oc} (V)	FF
Ref.	16.7	0.93	0.76
	16.4	0.95	0.78
HJ #1	15.9	0.73	0.63
	16.1	0.78	0.65
HJ #2	16.2	0.79	0.64
	16.5	0.87	0.68
HJ #3	16.9	0.98	0.76
	17.1	0.99	0.76
HJ #4	13.3	0.99	0.82
	13.2	0.99	0.82
HJ #5	13.7	0.99	0.80
	13.7	0.99	0.81

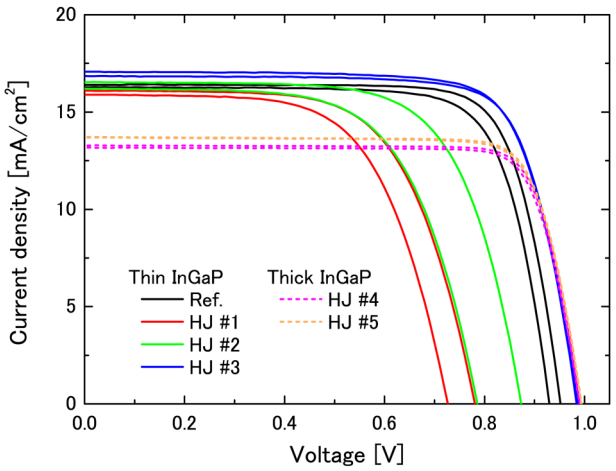

FIG. 5. LIV characteristics under AM1.5G (1 sun) illumination. The black solid line refers to the LIV of the reference cell. The other solid lines and dashed line refer to the LIV of heterojunction solar cells with a thin (50 nm) and thick (300 nm) InGaP emitter layer, respectively.

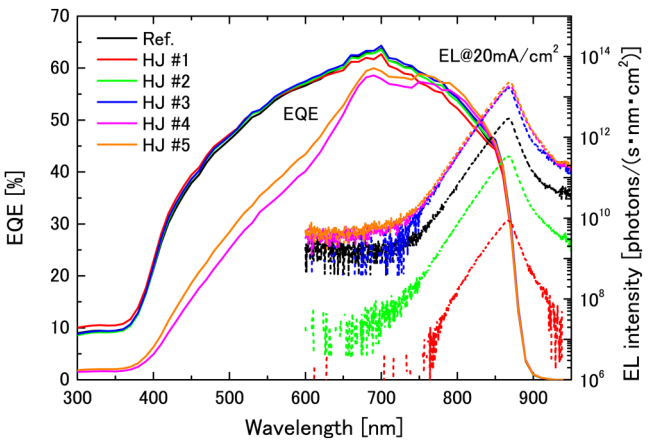

FIG. 6. The EQE spectra of the solar cells devices fabricated from the center area of the wafers. The absolute EL intensity spectra (broken curves) were obtained with an injected current density of 20 mA/cm^2.

the GaAs layer was observed. However, there is a significant sample dependence of the EL intensity of the GaAs layer. The EL intensities of HJ #1 and HJ #5 are 0.3% and 800% relative to that of the reference cell, respectively. Note that there is no emission from the InGaP layer. This indicates that the minority carrier density in the InGaP layer is much lower than that in the GaAs layer; that is, the effect of E_g of the InGaP emitter has a small effect on the electrochemical potential of the cell. If the quasi-Fermi-level splitting of the InGaP layer is larger than that of the GaAs layer, an additional EL signal of the InGaP layer may be observed, but such an InGaP/GaAs heterojunction solar cell cannot be regarded as a GaAs solar cell.

Figure 7 provides the DIV characteristics of the homojunction and heterojunction solar cells. The solid lines are the measurement results obtained using the SMU, and the symbols plot the function $V(J_{\mathrm{rec}})$ calculated by the following equation,[18] assuming that the reciprocity relation between EL and EQE is satisfied (this is verified below):

$$V(J_{\mathrm{rec}}) = V^{\mathrm{ideal}}(J_{\mathrm{rec}}) + \frac{kT}{q}\ln\frac{q\phi_{\mathrm{EL}}}{J_{\mathrm{rec}}}. \tag{4}$$

Here, V^{ideal} is the relation between V and J_{rec} that is obtained if the external luminescence efficiency η_{ext} is 100% (this function can be determined from the EQE spectrum) and ϕ_{EL} is the integrated EL intensity. Since the first and second terms on the right-hand side of Eq. (4) are calculated from the EQE and the EL intensity, respectively, the uncertainty of V can be derived from the measurement

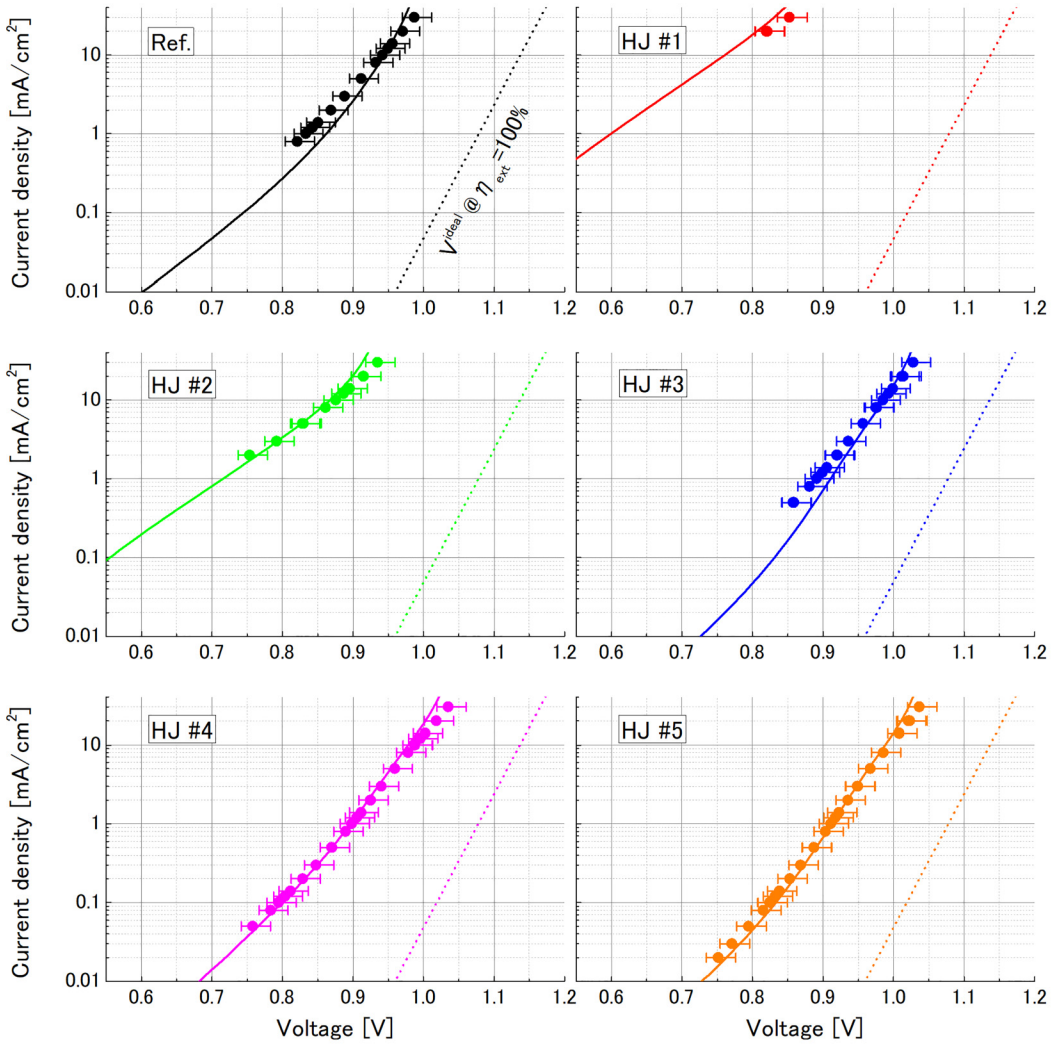

FIG. 7. IV characteristics of GaAs homojunction and InGaP/GaAs heterojunction solar cells under dark conditions. The measured and calculated values are shown with the solid curves and dot symbols, respectively. The dotted curves show the V^{ideal}, which corresponds to the case that the external luminescence efficiency is 100%.

uncertainty of the EQE and EL intensity. The error bars in Fig. 7 represent the uncertainty of V (K = 2) calculated using the law of the propagation of uncertainty.[17] We find that almost all measurement and calculation results agree within uncertainty (K = 2). By extending the coverage factor to 3, all calculation results are in agreement with the measurement values. This indicates that the reciprocity relation between EL and EQE is satisfied regardless of the structure of the solar cell. In other words, it is possible to discuss the differences in V_{oc} of the homojunction and heterojunction solar cells based on the EQE and EL characteristics: As shown in Fig. 6, all cells have the same EQE at the GaAs band edge, which has a strong effect on V^{ideal}. This means that there is essentially no difference in V^{ideal} among the samples, as shown by the dotted line in Fig. 7. On the other hand, the EL intensities of the GaAs layers are different. Therefore, we consider that the EL intensity of the GaAs layer explains the differences between the V_{oc} values shown in Table III. Table IV shows the saturation current densities obtained by fitting the $V(J_{rec})$ data to the following two-diode model:

$$J_{rec} = J_{01}\exp\left(\frac{qV}{kT}\right) + J_{02}\exp\left(\frac{qV}{2\,kT}\right). \tag{5}$$

Here, J_{01} and J_{02} are the contributions to the reverse saturation current density with diode factors of 1 and 2, respectively. In the case of HJ #1, J_{01} could not be obtained since J_{02} was too large. Table IV shows that there is no significant difference between the J_{01} values of the heterojunction solar cells except for HJ #1, and the reference cell has a larger value. J_{01} can be described by the following equation if we neglect the effect of surface recombination:

$$J_{01} = qn_i^2\left(\frac{D_n}{N_aL_n} + \frac{D_p}{N_dL_p}\right) + J_0^{rad}. \tag{6}$$

Here, D_n and D_p are the diffusion coefficients of electrons and holes, N_a and N_d are the acceptor and donor carrier densities, L_n and L_p are electron and hole diffusion lengths, and J_0^{rad} is the reverse saturation current density in the external radiative limit. Since all solar cells have similar V^{ideal} (that is, J_0^{rad}), as described above, it is considered that the low n_i of the InGaP emitter layer mostly contributes to the low J_{01} of the heterojunction devices. This suggests that the recombination loss in the neutral region of the emitter was reduced by using a heterojunction structure. Although J_{01} was the same in the heterojunction solar cells, we can confirm that a lower doping concentration of the emitter layer leads to a smaller J_{02}, which suggests a decrease in the nonradiative recombination current in the depletion region. We investigate the details below.

TABLE IV. Fitting results of the $V(J_{rec})$ with the two-diode model.

	J_{01} (A/cm^2)	J_{02} (A/cm^2)
Ref.	2.04×10^{-19}	9.02×10^{-11}
HJ #1	–	1.55×10^{-9}
HJ #2	6.32×10^{-20}	4.56×10^{-10}
HJ #3	7.14×10^{-20}	2.91×10^{-11}
HJ #4	4.35×10^{-20}	1.92×10^{-11}
HJ #5	5.72×10^{-20}	9.86×10^{-12}

To prove the theoretical prediction in Sec. II, we now determine the amount of SRH recombination in the depletion region of the different samples. Although the recombination in the depletion region is not directly accessible in the experiments, we can use the following approach: The total external luminescence efficiency of the device, η_{ext}, can be calculated from the measured EL intensity and J_{rec}. By considering the geometry of the solar cell allows us to derive the average internal luminescence efficiency of the whole cell volume, $\overline{\eta_{int}}$. The recombination in the depletion region determines the η_{int} in the depletion region, which in turn also contributes to $\overline{\eta_{int}}$. In particular, the J_{rec} dependences of $\overline{\eta_{int}}$ and η_{int} in the depletion region are reasonably equal if all carriers recombine in the depletion region.[6] Therefore, we compare the J_{rec} dependences of $\overline{\eta_{int}}$ (experimentally derived) and η_{int} (theoretically derived) to determine the range where all carriers recombine in the depletion region.

The closed circles in Fig. 8 show the dependences of $\overline{\eta_{int}}$ on J_{rec} for all samples. The error bars in Fig. 8 represent the uncertainty of $\overline{\eta_{int}}$ (K = 2).[17] $\overline{\eta_{int}}$ was evaluated using the following equation:[3]

$$\eta_{ext} = \frac{\overline{\eta_{int}}\,\overline{P_{esc}}}{1-\overline{\eta_{int}}\,\overline{P_{abs}}}. \tag{7}$$

Here, $\overline{P_{esc}}$ is the average probability for a photon to escape from the solar cell and $\overline{P_{abs}}$ is the average probability for photon absorption and the subsequent collection as photocurrent. These parameters are determined by the cell structure and can be derived numerically.[3] The obtained $\overline{\eta_{int}}$ data are compared with the results from Eq. (8) based on the AB model under the assumption of $n(x) = p(x) = n^{dep}$ in the depletion region,[6]

$$\eta_{int}^{dep} = \frac{Bn^{dep^2}}{\overline{A^{dep}}n^{dep} + Bn^{dep^2}}. \tag{8}$$

The AB model can be used to derive the η_{int} in the depletion region in GaAs (η_{int}^{dep}) based on the rate equations of the considered system. Since B is an intrinsic parameter [$B_{GaAs} = (1.7\pm0.2)\times10^{-10}$ cm^3 s^{-1}],[25] $\overline{A^{dep}}$ is the only free parameter that is left to fit the experimental n^{dep} (or J_{rec}) dependence of $\overline{\eta_{int}}$ to Eq. (8). We note that, in the low-J_{rec} regime in Fig. 8, the J_{rec} dependences of $\overline{\eta_{int}}$ coincide with the J_{rec} dependences of η_{int}^{dep} (the solid curves) in all devices. This indicates that all carriers recombine in the depletion region in the low-J_{rec} regime. Therefore, $\overline{A^{dep}}$ can be obtained by fitting $\overline{\eta_{int}}$ to Eq. (8) in the low-J_{rec} regime.[6] The fitting results of $\overline{A^{dep}}$ are shown in the figure. In the high-J_{rec} regime, $\overline{\eta_{int}}$ and η_{int}^{dep} are significantly different due to the influence of recombination in the neutral region.[6]

Figure 9 shows the correlation between the $\overline{A^{dep}}$ obtained in Fig. 8 and the average sulfur concentration in the InGaP emitter layer near the heterointerface shown in Fig. 4. The horizontal error bars (K = 2) represent the uncertainty in the SIMS measurement. The vertical error bars (K = 2) include the uncertainty of $\overline{\eta_{int}}$, B_{GaAs}, and n^{dep}. Figure 9 indicates that a lower sulfur concentration

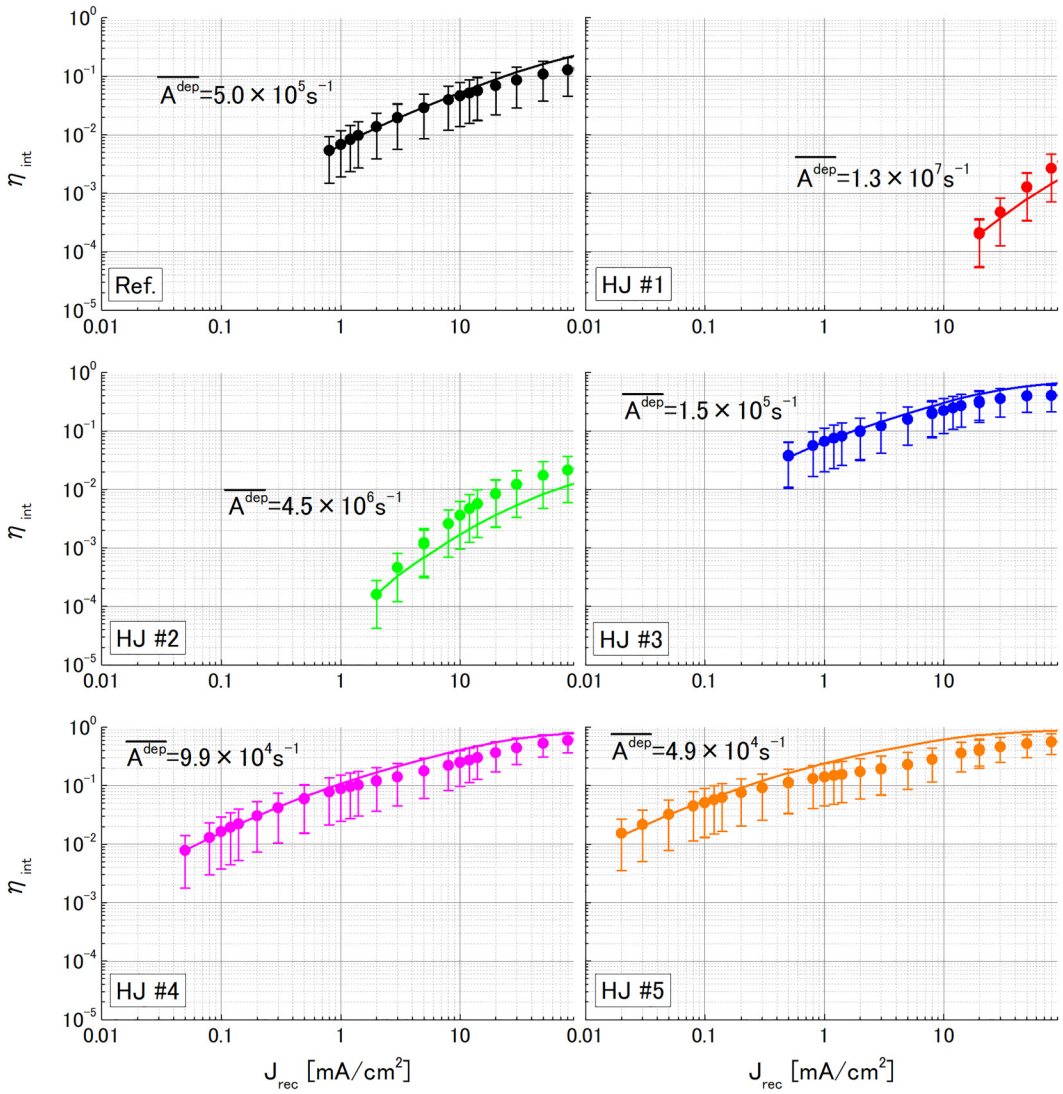

FIG. 8. Internal luminescence efficiencies of GaAs homojunction and InGaP/GaAs heterojunction solar cells as a function of the recombination current density. The measured and calculated values are shown with the symbols and solid curves, respectively. The values of $\overline{A^{dep}}$ given in the figure were obtained by fitting the data to Eq. (6).

in the InGaP layer results in a lower $\overline{A^{dep}}$ in the GaAs layer. This experimental result is consistent with the simulation result. We consider that the reduction in $\overline{A^{dep}}$ is not a result of a change in the material quality of GaAs since the design and growth conditions for the GaAs base layer were the same for all cells, and there was no difference in the EQE near the band edge of GaAs. Therefore, the reduction in $\overline{A^{dep}}$ in the regime of low sulfur concentrations in the InGaP layer is considered to be due to the reduction of U_{SRH} in the GaAs layer by controlling the position of the depletion region. Note that the values of $\overline{A^{dep}}$ of HJ #1 and HJ #2 are larger than those of the homojunction solar cell. This may be due to a decrease in the carrier lifetime in the GaAs near the heterointerface, such as considered in Cases 2 and 3 in the simulation. In the case of a significantly shorter lifetime in the GaAs near the heterointerface (Case 3), the $\overline{A^{dep}}$ of the heterojunction structure is higher than that of the homojunction structure even in the regime of low $n^{emitter}$ values. Since the $\overline{A^{dep}}$ values of HJ #3, HJ #4, and HJ #5 are lower than the $\overline{A^{dep}}$ of the homojunction solar cell, the qualities of the heterointerfaces in our solar cells are considered to be close to the condition of Case 2. By comparing the simulation results (Fig. 2) with the experimental results (Fig. 9), we find that there is a difference in the doping concentration that is required for low $\overline{A^{dep}}$ values. We believe that the reason for this difference is the local interdiffusion of sulfur and zinc at the heterointerface.

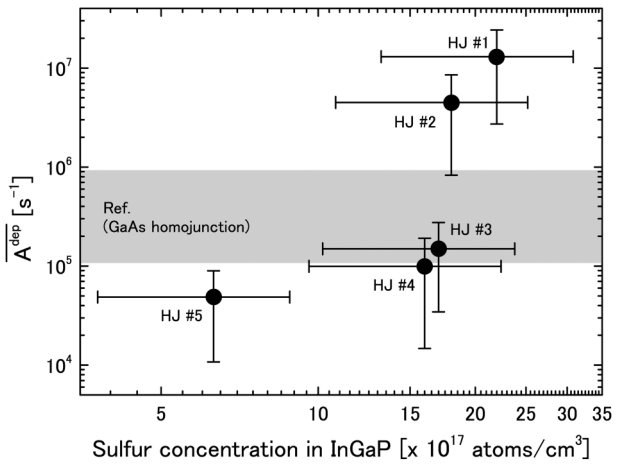

FIG. 9. Dependence of $\overline{A^{dep}}$ on the sulfur concentration in the InGaP layer. The gray area represents the range of $\overline{A^{dep}}$ in the GaAs homojunction solar cells.

However, a quantitative evaluation of local diffusion by SIMS is difficult due to the matrix effect in a mixed crystal and the knock-on effect at a p–n junction.[26] We consider that evaluating and controlling the interdiffusion of the dopants at the heterointerface is necessary to attain an optimized heterojunction structure.

In this study, we focused on front-junction devices in order to conveniently measure the EL spectrum of the wide-gap material. We believe that the effect of reducing the non-radiative recombination loss in the depletion region shown here for front-junction devices is one of the factors of the high conversion efficiencies realized by rear-junction devices.

V. CONCLUSIONS

We theoretically and experimentally investigated a method that can reduce the SRH recombination rate in the depletion region by solely modifying the solar cell structure without improving material quality. We have shown that $\overline{A^{dep}}$ can be reduced by employing a suitable heterojunction structure (with an emitter layer with a low intrinsic carrier concentration n_i) instead of a homojunction. In particular, $\overline{A^{dep}}$ can be improved by forming a significant part of the depletion region in the emitter layer, that is, by adjusting the doping concentration of the emitter layer to a level below that of the base layer. The reduction of $\overline{A^{dep}}$ is one of the reasons why a high η_{sc} can be achieved by a heterojunction structure. Our analysis suggests that, besides the quality of heterointerface, the combination of a low-n_i emitter layer material and a high-n_i base layer material can greatly contribute to the reduction of $\overline{A^{dep}}$. We believe that a further improvement of η_{sc} is possible by optimizing the heterointerface quality and the doping concentration profiles.

AUTHOR DECLARATIONS

Conflict of Interest

The authors have no conflicts to disclose.

DATA AVAILABILITY

The data that support the findings of this study are available from the corresponding author upon reasonable request.

REFERENCES

[1]M. Yamaguchi, K. Araki, K.-H. Lee, N. Kojima, T. Masuda, K. Kimura, A. Satou, and H. Yamada, in *Proceedings of the 5th IEEE International Conference on Smart Energy Grid Engineering, Oshawa, ON, Canada, 14–17 August 2017* (IEEE, 2017), pp. 394–399.
[2]M. Yamaguchi, T. Masuda, K. Araki, D. Sato, K.-H. Lee, N. Kojima, T. Takamoto, K. Okumura, A. Satou, K. Yamada, T. Nakado, Y. Zushi, M. Yamazaki, and H. Yamada, Energy Power Eng. **12**, 375 (2020).
[3]M. A. Steiner, J. F. Geisz, I. García, D. J. Friedman, A. Duda, and S. R. Kurtz, J. Appl. Phys. **113**, 123109 (2013).
[4]L. Zhu, T. Mochizuki, M. Yoshita, S. Chen, S. Sato, C. Kim, H. Akiyama, and Y. Kanemitsu, in *Proceedings of 40th IEEE Photovoltaic Specialist Conference, Denver, CO, 8–13 June 2014* (IEEE, 2014), pp. 3404–3408.
[5]J. F. Geisz, M. A. Steiner, I. García, R. M. France, D. J. Friedman, and S. R. Kurtz, IEEE J. Photovolt. **5**(1), 418 (2015).
[6]T. Nakamura, M. Imaizumi, H. Akiyama, and Y. Okada, Prog. Photovolt. Res. Appl. **28**(5), 417 (2020).
[7]W. Shockley and W. T. Read, Phys. Rev. **87**(5), 835 (1952).
[8]R. N. Hall, Phys. Rev. **87**(2), 387 (1952).
[9]C.-t. Sah, R. N. Noyce, and W. Shockley, Proc. IRE **45**(9), 1228 (1957).
[10]S. De Wolf, A. Descoeudres, Z. C. Holman, and C. Ballif, Green **2**, 7 (2012).
[11]A. B. Slimane, A. Michaud, A. Bercegol, J. Goffard, O. Mauguin, X. Lafosse, K. Saliou, L. Lombez, J.-C. Harmand, and S. Collin, in *Proceedings of 46th IEEE Photovoltaic Specialist Conference, Chicago, IL, 16–21 June 2019* (IEEE, 2019), pp. 3219–3223.
[12]S. Heckelman, D. Lackner, C. Karcher, F. Dimroth, and A. W. Bett, IEEE J. Photovolt. **5**(1), 446 (2015).
[13]F. W. Ragay, E. W. M. Ruigrok, and J. H. Wolter, in *Proceedings of 1st World Conference on Photovoltaic Energy Conversion, Waikoloa, HI, 5–9 December 1994* (IEEE, 1994), pp. 1934–1937.
[14]M. A. Steiner, R. M. France, E. E. Perl, D. J. Friedman, J. Simon, and J. F. Geisz, IEEE J. Photovolt. **10**(2), 487 (2020).
[15]J. F. Geisz, M. A. Steiner, I. García, S. R. Kurtz, and D. J. Friedman, Appl. Phys. Lett. **103**, 041118 (2013).
[16]S.-T. Hwang, S. Kim, H. Cheun, H. Lee, B. Lee, T. Hwang, S. Lee, W. Yoon, H.-M. Lee, and B. Park, Sol. Energy Mater. Sol. Cells **155**, 264 (2016).
[17]T. Nakamura, L. Zhu, M. Yoshita, M. Imaizumi, H. Akiyama, and Y. Okada, in *Proceedings of 7th World Conference on Photovoltaic Energy Conversion, Waikoloa, HI, 10–15 June 2018* (IEEE, 2018), pp. 921–926.
[18]U. Rau, Phys. Rev. B **76**, 085303 (2007).
[19]J.-I. Shim, D.-P. Han, C.-H. Oh, H. Jung, and D.-S. Shin, J. Quantum Electron. **54**(2), 8000106 (2018).
[20]See https://www.engineering.unsw.edu.au/energy-engineering/research/software-data-links/pc1d-software-for-modelling-a-solar-cell for information about PC1D; accessed 28 December 2020.
[21]C. L. Schilling, O. Höhn, D. N. Micha, S. Heckelmann, V. Klinger, E. Oliva, and S. W. Glunz, J. Photovolt. **8**(1), 348 (2018).
[22]H. Fujikura, A. Hirama, F. Ishikawa, H. Sai, and H. Hasegawa, in *Proceedings of International Conference on Indium Phosphide and Related Materials, Williamsburg, VA, 14–18 May 2000* (IEEE, 2000), pp. 372–375.
[23]S. Sato, T. Oshima, and M. Imaizumi, J. Appl. Phys. **105**, 044504 (2009).
[24]M. Yoshita, L. Zhu, C. Kim, H. Kubota, T. Nakamura, M. Imaizumi, Y. Kanemitsu, and H. Akiyama, in *Proceedings of 43rd IEEE Photovoltaic Specialists Conference, Portland, OR, 5–10 June 2016* (IEEE, 2016), pp. 3570–3573.
[25]U. Strauss and W. W. Rühle, Appl. Phys. Lett. **62**(1), 55 (1992).
[26]E. Zinner, J. Scanning Microsc. **3**(2), 57 (1980).